Miami A. Mohammed [1]
Ahmad K. Ahmad [2]

[1] Department of Physics, College of Science, University of Al-Mustansiriyah, Baghdad, IRAQ
[2] Department of Laser and Optoelectronics Engineering, College of Engineering, Al-Nahrain University, Baghdad, IRAQ

Femtosecond Laser Writing of Photonic Crystal in $LiNbO_3$ Crystal

A numerical investigation of depressed cladding photonic crystal that has been buried in bulk lithium niobate crystal material by direct femtosecond laser writing. The leading guide of light propagation is elucidated through the photonic crystal that is embedded in a lithium niobate. The induced refractive index, confinement losses, and dispersion are numerically calculated according to the orientation of the crystal and the structure geometry of the photonic crystal. This structure supports single and highly multimode transverse electric and transverse magnetic wave guidance at the communication wavelength 1.55 μm. We realized that the confinement losses are less than 1 dB/cm for both polarizations, and the transmission properties appear good for several photonic crystal applications.

Keywords: $LiNbO_3$ crystal; Photonic crystal; Optical waveguides; Laser materials
Received: 27 February 2025; **Revised:** 28 April 2025; **Accepted:** 4 May 2025

1. Introduction

An optical waveguide consists of the dielectric material called the core that has a refractive index (RI) n_1 surrounded by another dielectric material called cladding or substrate that has a lower refractive index n_2, it's operated according to total internal reflection condition $n_1>n_2$, the light will stay confined inside the core region of the waveguide [1-4]. Several techniques are used for the fabrication of waveguide structures like thermal ion implantation, ion in-diffusion, ion/proton exchange, and laser femtosecond (fs) micromachining [5-8]. Recently, fs-laser micromachining has become one of the most efficacious techniques used in 3D volume transparent material microstructure, the fs-laser micromachining technique has been exceedingly used to make optical waveguides from dissimilar materials like glasses, crystals, ceramics, and polymers [9-12]. When the high-intensity fs laser beam focuses inside the transparent crystal, some of the modification happens in the modified region due to a change in the optical properties to induce the refractive index modulations. Femtosecond laser direct micromachining writing techniques used for the fabrication of arbitrary shapes waveguide structures in bulk of the different crystalline materials are considered a challenging task [9-10]. This micromachining permits to design of integrated optical devices with a great degree of freedom such as buried integrated laser sources, single-photon detectors, amplifiers, nonlinear-frequency converters, etc. [9]. It is possible to create Type I directly written optical waveguides, Type II stress-induced waveguides, and Type III depressed cladding waveguides by utilizing fs-laser micromachining [11-14].

Type I waveguides are inserted inside the fs laser-induced tracks and then fs-laser-induced positive refractive-index changes $\Delta n>0$ in the focal volume region. This positive change of the refractive index is very public in amorphous materials like the glasses [13], Type I waveguides are made at low pulse energies just above the modification threshold [10]. Additionally, crystal-generated Type I waveguides can only provide polarization guidance in one direction, limiting their ability to perform phase-matched frequency conversion, which requires 2D guidance. [13], i.e., increasing the characteristic of E extraordinary polarization than the O ordinary polarization, besides reducing the nonlinear response [10].

The surrounding areas of fs laser-induced tracks frequently contain Type II waveguides, where they cause negative refractive index shifts $\Delta n<0$ directly in the exposed area, causing the lattices in the focus volume to grow and occurring extension of the core area usually due to reduction in the refractive index, while the nearby areas might have a comparatively higher index due to the stress-induced effects. Type II waveguides are created because high pulse energy causes significant harm to the crystalline structure. In addition, the focal region's crystal lattice may be broken, resulting in a decrease in the refractive indices for both O and E polarization. Moreover, the stress fields produce an increase of the adjusted volume region and then spread over the nearby regions, causing local alterations in the refractive indices, which are enhanced in either the ordinary or extraordinary index direction where the direction of the stress depends on it, and this led to the type II modification [10]. Yet, the dual line waveguide geometry in crystals is typically

the most popular way due to the stress-induced and produces in the irradiated tracks changes of negative refractive index [10-13].

Type III waveguides include depressed cladding waveguides which recently have attracted much attention as well [11]. Depressed cladding is formed from a waveguide core surrounded by several low index cladding tracks, the position of the core is slightly away from the tracks and the separation distance between the tracks is close to each other (a few μm). This structure is a quasi-continuous low-index potential barrier wall permitting light confinement inside it [12]. More importantly, the possibility of manufacturing different diameters and shapes with all the flexibility of the waveguide cores cross section which makes the depressed cladding enables to guide the light from visible to mid-IR wavelength ranges and from single mode to highly multimode. Further, in a 3D vision, where the morphology of 2D waveguide cladding appears as the guiding tube, making the depressed cladding allows an excellent interconnection with other commercial fibres for the construction of fiber-waveguide-fiber integrated photonic systems, supporting the guidance to the longer wavelength region [11-13]. A very important aspect of 2D waveguide cladding cross-section in most crystals may support the guidance which is very much identical along TE and TM polarizations [11-13].

Lithium niobate ($LiNbO_3$) crystalline material has unique properties such as the combination between nonlinear optical properties (χ^2), birefringence, electro-optical, acoustic optical, and broad transparency window, all these properties make the $LiNbO_3$ crystal an attracting material in many applications of integrated optics [9-10]. As well as $LiNbO_3$ crystals is a negative uniaxial birefringent crystal and appropriate for different types of waveguide fabrication like type I and type II as type I single tracks. $LiNbO_3$ crystals appear to have good waveguiding properties and induce positive RI contrasts which are normally induced by direct fs laser writing [10], and dual-line tracks where the guidance happens only in the surrounding regions. As a result of the residual stress, this feature has a lower refractive index in the middle region route and a bit higher RI in the close by vicinity [10,13]. These dual-line tracks are the most basic sort of depressed-index cladding, consisting of merely two parallel routes separated by a small distance (μm). However, such a structure does not permit controlling of the guiding characteristics. The depressed cladding structure of type III waveguides has an advantage over type II waveguides in that it comprises a lot of cladding tracks that are positioned randomly (circular, triangular, and hexagonal) and this enables guiding the light and ensures a good confinement in the core region to longer wavelength regions having lower propagation losses than single-track written [3,9,11,15-20].

In this study, we investigate numerically with the aid of the finite element method, using the COMSOL Multiphysics software, the depressed cladding of a photonic crystal buried in a z-cut bulk $LiNbO_3$ crystal by fs-laser writing. The shape and size of the structure of the cladding and how it affects the guiding properties, the variance between the refractive index of low–index cladding structure, and the slightly high-core guiding index are all analyses. The propagation constants of modes, confinement loss, and dispersion with different polarizations are also studied. The anisotropic material and material absorption can be described by the COMSOL program using a perfect match layer PML absorber that surrounds the PC cross-section.

2. Theoretical Part

A numerical simulation by COMSOL Multiphysics is applied to design 2D depressed cladding of photonic crystal (PC) with a hexagonal lattice consisting of five rings about 91 holes, have pitches $\Lambda = 5\ and\ 7\ \mu m$, and a hole diameter ($d_{hole}$=4.48μm), which is different from reference [9]. This cladding can be written by direct fs-laser in bulk of the z-cut $LiNbO_3$ crystal, z-cut $LiNbO_3$ is parallel to the crystal optical axis. Assuming that the light is propagated in the y-axis as displayed in Fig. (1). However, the refractive index contrast via the cross-section takes a negative sign of every track of cladding and the lattice cladding with five rings leads to a decrease of the losses for each of ordinary O and extraordinary E polarizations better than one or two rings. The indices according to Sellmeier expansions for 5 mol.% magnesium oxide MgO doped LiNbO3 is a negative uniaxial crystal where $n_e<n_o$ [9,21]. In a simulation using COMSOL software, the frequency-domain electromagnetic-wave model was used for the guiding mode analysis at the wavelength 1.55 μm. By applying the wave equation for optical monochromatic waves, in a non-magnetic anisotropic optical region, having an angular frequency ω, and a relative permittivity $\hat{\varepsilon}$, the electric field vector (E) wave equation eq. (1) becomes as follows [9,21,22]:

$$\nabla \times (\nabla \times \boldsymbol{E}) - k_\circ^2 \hat{\varepsilon}_r \varepsilon_\circ \Rightarrow \nabla^2 \boldsymbol{E} - \omega^2 \mu_\circ \varepsilon_\circ \hat{\varepsilon}_r \boldsymbol{E} = 0 \quad (1)$$

where both $\varepsilon_\circ$ and $\mu_\circ$ are represent the vacuum permittivity and permeability respectively, $\exp(i\omega t)$ is the time dependence factor

For transparent $LiNbO_3$ uniaxial crystal, and the dielectric tensor $\hat{\varepsilon}_r$ can be described as:

$$\mathcal{E}_r = \begin{pmatrix} \mathcal{E}_o & 0 & 0 \\ 0 & \mathcal{E}_0 & 0 \\ 0 & 0 & \mathcal{E}_e \end{pmatrix} \quad (2)$$

where $\hat{\varepsilon}_r = (n_{o,e} + \delta n)^2$, and $(n_{o,e})$ represents the refractive indices of the O and E for the uniaxial crystal domain. The δn is non-zero only in the irradiated domain [9]. COMSOL program is used to solve Equations 1 and 2 to calculate the propagation constant mode and the effective index of the two states of the

orthogonal polarization in the x- and z-directions as $n_{0,e}^{eff} = \beta_{o,e}/k_0$, where k_0 is the free-space wave number ($k_0 = 2\pi/\lambda$). The effective index n_{eff} is a complex value that contains real and imaginary parts, the imaginary part of the n_{eff} is related to the confinement loss (dB/cm) as:

$$L = 40\pi\, Im(n_{eff}) \times 10^4/[\lambda\ (\mu m) Ln(10)] \quad (3)$$

While the real part is related to dispersion parameters according to the formal of chromatic dispersion, the waveguide dispersion connected to the structure as well as the PC dispersion that is elevated from the unmodified material dispersion can be expressed as follows [9,21,22]:

$$D = -(\lambda/c)\partial^2(n_{eff})/\partial\lambda^2 \quad (4)$$

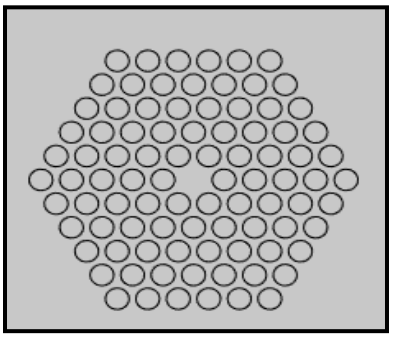

(a) $\Lambda = 7\mu m$

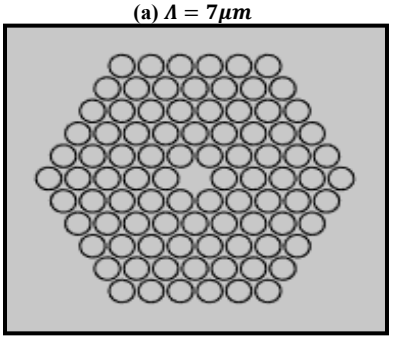

(b) $\Lambda = 5\mu m$

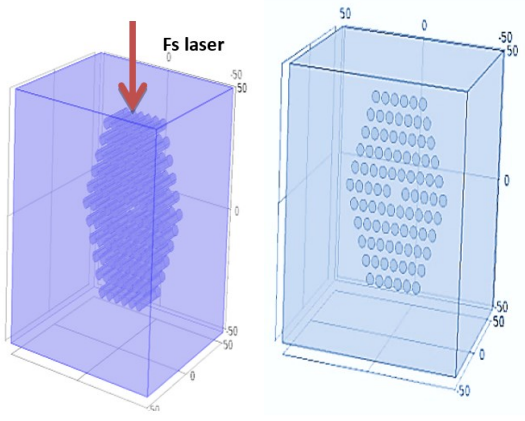

(c) **(d)**

Fig. (1) Modeled 2D depressed cladding of PC with a hexagonal lattice, five rings (a) $\Lambda = 7\mu m$ (b) $\Lambda = 5\ \mu m$, and ($d_{hole} = 4.48\ \mu m$) buried in bulk $LiNbO_3$ crystal, (c) view of 2D PC cross-section embedded in $LiNbO_3$ Crystal using fs-laser writing and (d) PCF cross-section

In our numerical simulations using the perfectly matched layer (PML) (Fig. 2), the fundamental concept of the PML is that, by use of impedance matching and anisotropic damping, it operates as an absorbing, reflectionless medium that permits waves to leave the computational domain without introducing artefacts. Proper implementation (thickness, absorption profile, and numerical discretisation) is necessary for its efficacy. Isotropic and rectangular PML surrounding PC structure cross-section are used in our, with free triangular mesh and maximum mesh size was 0.53 µm at the domain's edge, and minimum mesh size was 0.024 µm in the domain's core, with a relative growth rate of 1.33.

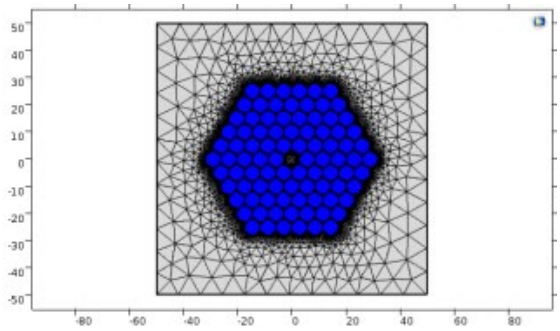

Fig. (2) PML that is surrounding PC structure with free triangular mesh and maximum mesh size was 0.53 µm at the domain's edge, and minimum mesh size was 0.024 µm in the domain's core, with a relative growth rate of 1.33

3. Results and Discussion

After using COMSOL software to model the light propagation through two-dimensional photonic crystal buried in three dimensions $LiNbO_3$, to find the mode propagation constants and the effective index of the two orthogonal polarizations O and E, at the wavelength 1.55 µm and according to the crystalline orientations. Also, fs laser written depressed cladding in crystal material includes changes in refractive index are increased and decreased in volumes of material. As well as, the changes in the refractive index are negative signs via a cross-section of each track. The numerical results for PC with pitches (Λ =5 µm and 7µm) and hole diameter d_h=4.48µm as displayed in the (Fig. 3 and Fig. 4). First, the refractive index contrast is typically 10^{-3}-10^{-2} for example Δn=-1.02x10^{-3}, Δn=-1.08x10^{-3}, Δn=-2.1x10^{-2}, and Δn=-1x10^{-2} for polarization n_e while for n_o polarization are Δn=3.2x10^{-3}, Δn=-4.4x10^{-3}, Δn=-2.3x10^{-2} and Δn=-1.2x10^{-2}. For both modes, the variation of the refractive index of the extraordinary polarization is lower than the ordinary polarization in both cases, this indicates slightly stronger guiding properties along O than E polarizations. Second, one can see the distribution of the field modal for 2D PC depressed cladding in $LiNbO_3$ at the wavelength 1.55µm is highly multimode.

Figure (3) shows the pitch Λ =5μm, the field modal distributions along the extraordinary index (n_e) polarization including the images (f, g, h, l, m, o, r, s, t, u and v) and in (f1, g1, h1, l1, m1, o1, r1, s1,t1, u1 and v1) for the TE and TM polarization modes for the TE and TM polarizations mode while the other polarizations are along the ordinary index (n_o) were included. While figure (4) shows the pitch (Λ =7μm), the field modal distributions of PC in $LiNbO_3$ are along the extraordinary index (n_e) polarization includes images (b, e, k, i, n, p, s and u) and (b1, e1, k1, i1,, n1 , p1, s1 and u1) for the TE and TM polarizations mode while the others polarization are along the ordinary index (n_o). Third, the guiding shows a single mode distribution for both polarization (TE and TM) only in o and o1 as in Fig. (3), and in a and a1 as in Fig. (4), while the guiding is highly multimode in the others involves the potential for effective guiding by fs laser at the wavelength 1.55 μm region of $LiNbO_3$. Fourth, from the two figures, in most cases shows featuring induce an increase or decrease refractive index in the central region of the PF while highly or slightly increase refractive index in the surrounding regions for both pitchers 5 μm and 7μm. Fifth, depressed cladding has been confirmed to be a good mode confinement and reduction losses in O and E polarizations includes identical tracks.

This study shows the results for guidance along both refractive indexes the polarization n_o and n_e represented the best approach and a good method can be considered for further comparison with the works achieved previously on a $LiNbO_3$ crystal, where shown from references [10,15,23]. Waveguides of Type I only guide the E index (n_e) polarization and Type II waveguides are along both polarizations (n_o) and (n_e), even though the guidance along n_o was weaker [10,15] and nearly agree with the study that is achieved in ref [23]. Figure (5) represents the variation in the real part of effective indices of the unmodified material for both O and E waves with the wavelength for PC five hexagonal rings with d_{hole}=4.48μm and Λ=5μm embedded in $LiNbO_3$ crystal. Also, shows the numerical results where the real part of the effective refractive index of the ordinary n_o^{eff} is slightly greater than n_e^{eff} the extraordinary PC, as well as the refractive indices of the unmodified material n_o is also, slightly greater n_e. By increasing the wavelength, the difference between the rear parts of effective indices and the refractive indices of both O and E waves is increased. Note from Fig. (5), the curves of effective indices of both O and E waves are deviation from the refractive indices of both O and E waves especially from the wavelengths 0.7 to 1.6 μm. Due to increasing the wavelength towards the long wavelengths, the confinement of modes is decreased. While, at the short wavelength the confinement of modes increased and the difference between the refractive index are almost nonexistent.

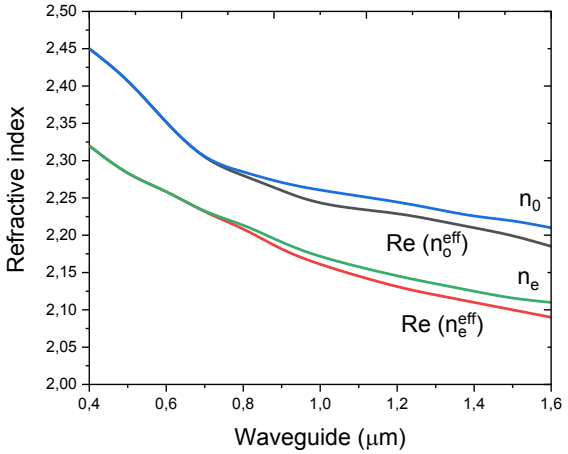

Fig. (5) Variation of refractive indices and real parts of effective indices of unmodified material for both O and E waves with wavelength, for five hexagonal rings PC with d_{hole}=4.48μm and Λ=5μm

Also, the confinement loss mode and the dispersion that is considered the crucial features of PC can be controlled by the geometry of lattice rings and structure parameter (diameter of holes and pitch) which have the important effects on the PC characteristics as shown in Fig. (6) and Fig. (7).

The confinement loss mode is considered an important parameter for any geometry design of PC and is intrinsically related to the waveguide geometry. Figure (6) demonstrates the relationship between the wavelength and the confinement losses of the E and O polarizations for the PC with the two distinct pitches 5 and 7 μm. The results demonstrate that the confinement loss modes in both O and E polarizations are smaller than 1dB/cm and this level of the losses is reasonable for many technological applications. Also, when increasing the pitch to 7 μm, the loss in both O and E polarizations are more than that for 5 μm, whereas at the shorter wavelengths, the losses are nearly raised for the pith 7 μm than 5 μm but when reaching wavelengths near 1.55 μm the losses of pitch 7 μm become lower than that for pitch 5 μm. Figure (6) also shows that a reduction of the losses of the E polarizations is about 10^{-4} for pitch 5 μm and 10^{-6} for pitch 7 μm near the wavelength 1.55 μm. Whereas, for the O polarizations are about 10^{-1} for pitch 5 μm and 10^{-2} for pitch 7 μm, these results are significant for many applications of waveguide structures. In addition, at the lower wavelengths there are different behaviors of both the O and E polarizations confinement losses than that in longer wavelength. The resonance behavior in anisotropic waveguides is caused by the fundamental mode coupling of E polarization to the radial mode of O polarization and subsequent E wave leakage via O modes. Additionally, there are many propagating modes losses through the structure because of various

parameters that cause the losses to be high. Such losses result from the material absorption caused by the fs-laser, as well as the scattering losses resulting from the cladding tracks' imperfections (non-smoothness), as well as the imperfect locating of the tracks due to enhancing the mode leakage from the guiding region. The results are somewhat close to the references [9,21,24] despite different construction and engineering parameters, as well as, extending up to the wavelengths longer than 1.55 µm for optimization; this indicates the validity of the performance.

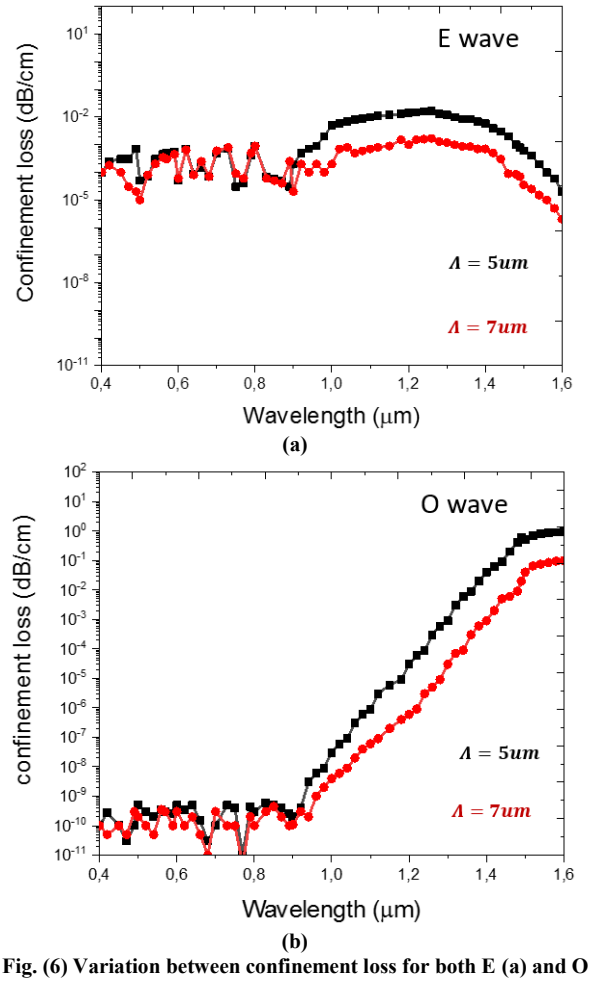

Fig. (6) Variation between confinement loss for both E (a) and O (b) polarizations versu wavelength under two pitches 5µm and 7µm, for five rings PC

The numerical results presented in Fig. (7) show the dispersion curves at a smaller pitch 5 µm are very pronounced than for pitch 7 µm, the dispersion changes are due to waveguide dispersion and this change has no big effect on the total structure dispersion. For shorter wavelengths, the mode is more confined and guiding in the core region, while at the longer wavelengths the guidance is poorer, and modes become as the leaky modes because these modes are none of the resonance features resulting from the periodicity of the structure.

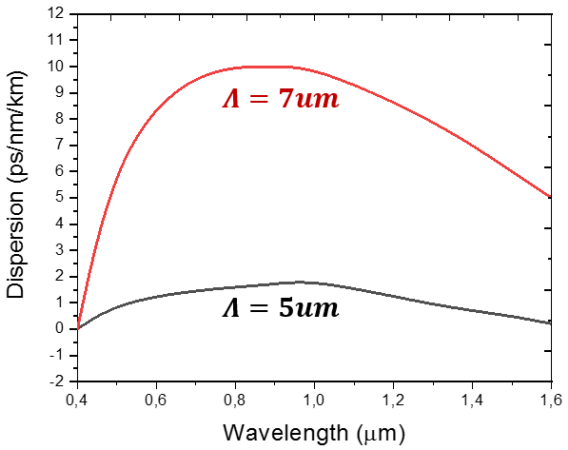

Fig. (7) Variation of dispersion with wavelength for O waves

4. Conclusion

A numerical simulation has been presented a hexagonal PC lattice embedded in 3D $LiNbO_3$ crystal by direct fs-laser writing for supporting the guidance along n_e and n_o plarizations at the wavelength 1.55 µm. The guiding properties for both O and E polarizations, the effective refractive index, the confinement losses, and dispersion for two different pitches are calculated using COMSOL software. A reliable performance achieved using cladding layers formed from five hexagonal rings for two different pitches for both of single and highly multimode for TE and TM polarization considering the crystalline orientations and the optimum design for coupling PC fiber in the future. The minimum loss is less than 1 dB/cm, where the losses reduction is in both the O, and the E polarizations. The E polarization losses are more than three orders less than in the O polarization losses according to pitch that is used near the telecommunication wavelength 1.55 µm. These results promise good transmission features by using $LiNbO_3$ crystal in application for waveguide guiding coupling in the integrated optical devices.

References

[1] G.A. Reider, **"Photonics: An Introduction"**, Springer (2016).

[2] Y. Jia, Sh. Wang and F. Chen, "Femtosecond laser direct writing of flexibly configured waveguide geometries in optical cryst als: fabrication and application", *J. Opto-Electron. Adv.*, 3(10) (12020) 1-12.

[3] L. Li, W. Kong and F. Chen, "Femtosecond laser-inscribed optical waveguides in dielectric crystals: a concise review and recent advances", *J. Adv. Photon.*, 4(2) (2022) 1-29.

[4] C. Grivas, "Optically pumped planar waveguide lasers, Part I: Fundamentals and fabrication

techniques", *Prog. J. Quant. Electron.,* 35(6) (2011) 159–239.

[5] D. Jaque, E. Cantelar and G. Lifante, "Lattice micro-modifications induced by Zn diffusion in Nd:$LiNbO_3$ channel waveguides probed by Nd^{3+} confocal micro-luminescence", *J. Appl. Phys.*, B88(2) (2007) 201–204.

[6] F. Chen, "Micro-and submicrometric waveguiding structures in optical crystals produced by ion beams for photonic applications", *J. Laser Photon. Rev.*, 6(5) (2012) 622–640.

[7] A. Tervonen, B.R. West and S. Honkanen, "Ion-exchanged glass waveguide technology: a review", *J. Opt. Eng.*, 50(7) (2011) 071107.

[8] G. Della, R. Osallame and P. Laporta "Micromachining of photonic devices by femtosec-ond laser pulses", *J. Opt. A: Pure Appl. Opt.*, 11 (2009), 1-18 (013001).

[9] H. Karakuzu, M. Dubov and S. Boscolo, "Control of the properties of micro-structured waveguides in lithium niobate crystal", *Opt. Exp.*, 21 (2013) 17122-17130.

[10] R. Osellame, G. Cerullo and R. Ramponi, "Femtosecond Laser Micromachining: Photonic and Microfluidic Devices in Transparent Materials", Topics in Applied Physics 123 Springer-Verlag (2012).

[11] R. He et al., "Femtosecond laser micromachining of lithium niobate depressed cladding waveguides", *Opt. Mater. Exp.*, 3(9) (2013) 1378-1384.

[12] Y. Tian et al., "A Brief Review on Nonlinear Photonic Crystals Induced by Direct Femtosecond Laser Writing", *Photonics*, 10(833) (2023) 1-22.

[13] F. Chen and J.R. Vázquez de Aldana, "Optical waveguides in crystalline dielectric materials produced by femtosecond-laser micromachining", *J. Laser Photon. Rev.*, 8(2) (2014) 251-275.

[14] B. Zhang, L. Wang and F. Chen, "Recent Advances in Femtosecond Laser Processing of LiNbO3 Crystals for Photonic Applications", *J. Laser Photon. Rev.*, 14(8) (2020) 1900407.

[15] J. Burghoff, S. Nolte and A. Tunnermann, "Origins of waveguiding in femtosecond laser-structured $LiNbO_3$", *J. Appl. Phys.*, A89 (2007) 127–132.

[16] A. Okhrimchuk et al., "Low loss depressed cladding waveguide inscribed in YAG:Nd single crystal by femtosecond laser pulses", *Opt. Exp.*, 20 (2012) 3832–3843.

[17] Q. An et al., "Mid-infrared waveguides in zinc sulfide crystal", *Opt. Mater. Exp.*, 3 (2013) 466–471.

[18] L. Dong, W. Wong and M. E. Fermann, "Single-mode propagation in fibers and rods with large leakage channels", Patent US 2013/0089113 A1 (2013). http://www.google.co.uk/patents/US7787729.

[19] O.A. Hammadi and M.S. Edan, "Temperature Dependencies of Refractive Index and Optical Elasticity Coefficient on Lens Induced in Nd:YAG Crystal", *Iraqi J. Appl. Phys.*, 8(1) (2012) 35-41.

[20] F. Chen, "Recent advances on femtosecond laser writing of waveguides in crystals", *Proc. Vol., Front. in Ultrafast Optics: Biomed. Sci. Indust. Appl. XXI*, 1167619 (2021).

[21] H. Karakuzu et al., „Optimization of microstructured waveguides in z-cut $LiNbO_3$ crystals", *Opt. Exp.*, 4(3) (2014) 541-552.

[22] J.-F. Lee, "Full-Wave Analysis of Dielectric Waveguides Using Tangential Vector Finite Elements tics", *IEEE Trans. Microwave Theory Tech.*, 39(8) (1991) 1262-1271.

[23] J. Thomas et al., "Laser direct writing: Enabling monolithic and hybrid integrated solutions on the lithium niobate platform", *phys. stat. sol. a*, 208(2) (2011) 276–283.

[24] Y. Shen et al., "Femtosecond laser writing of waveguides in zinc oxide crystals: fabrication and mode modulation", *Opt. Exp.*, 30(15) (2022) 27694-27703.

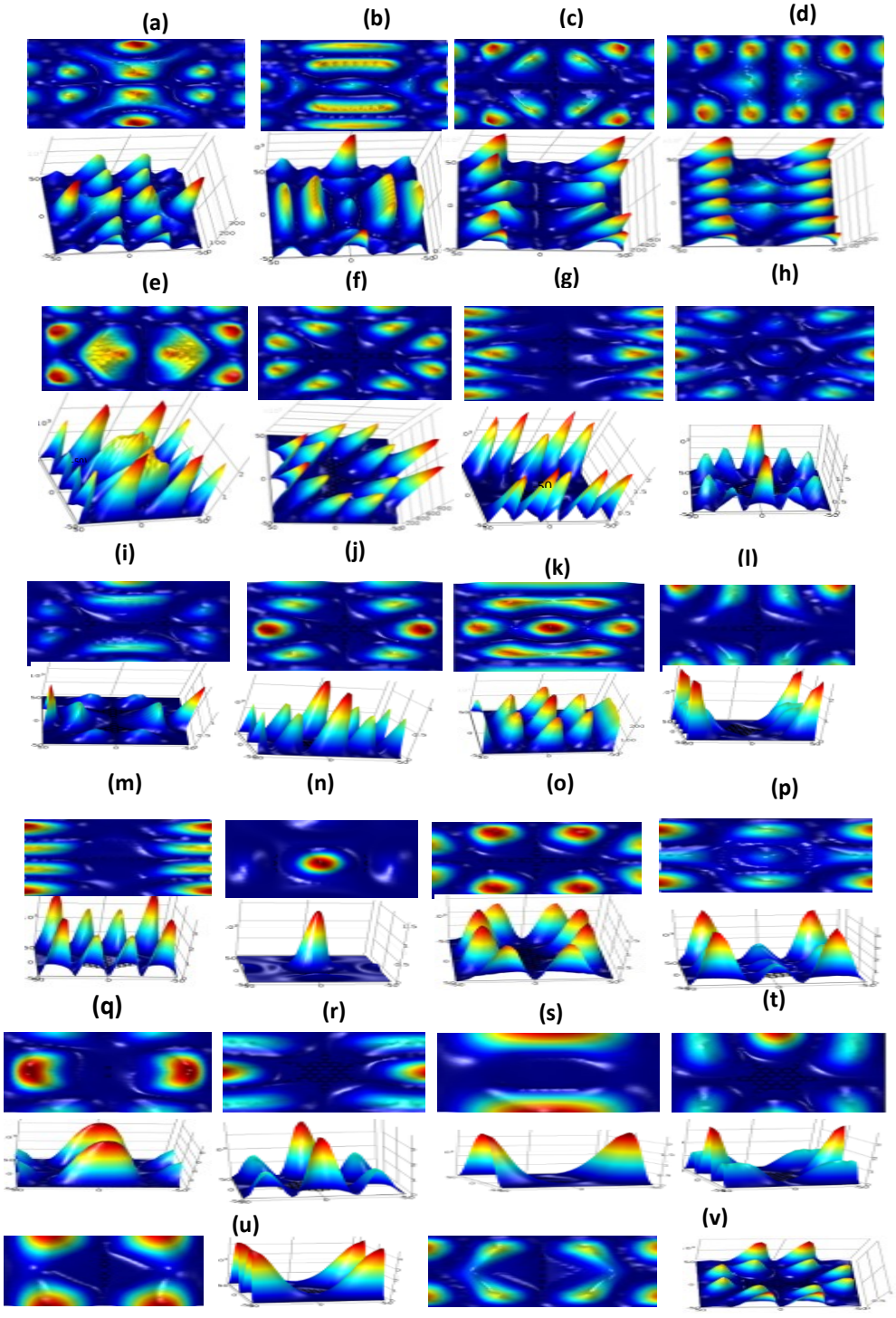

(A)

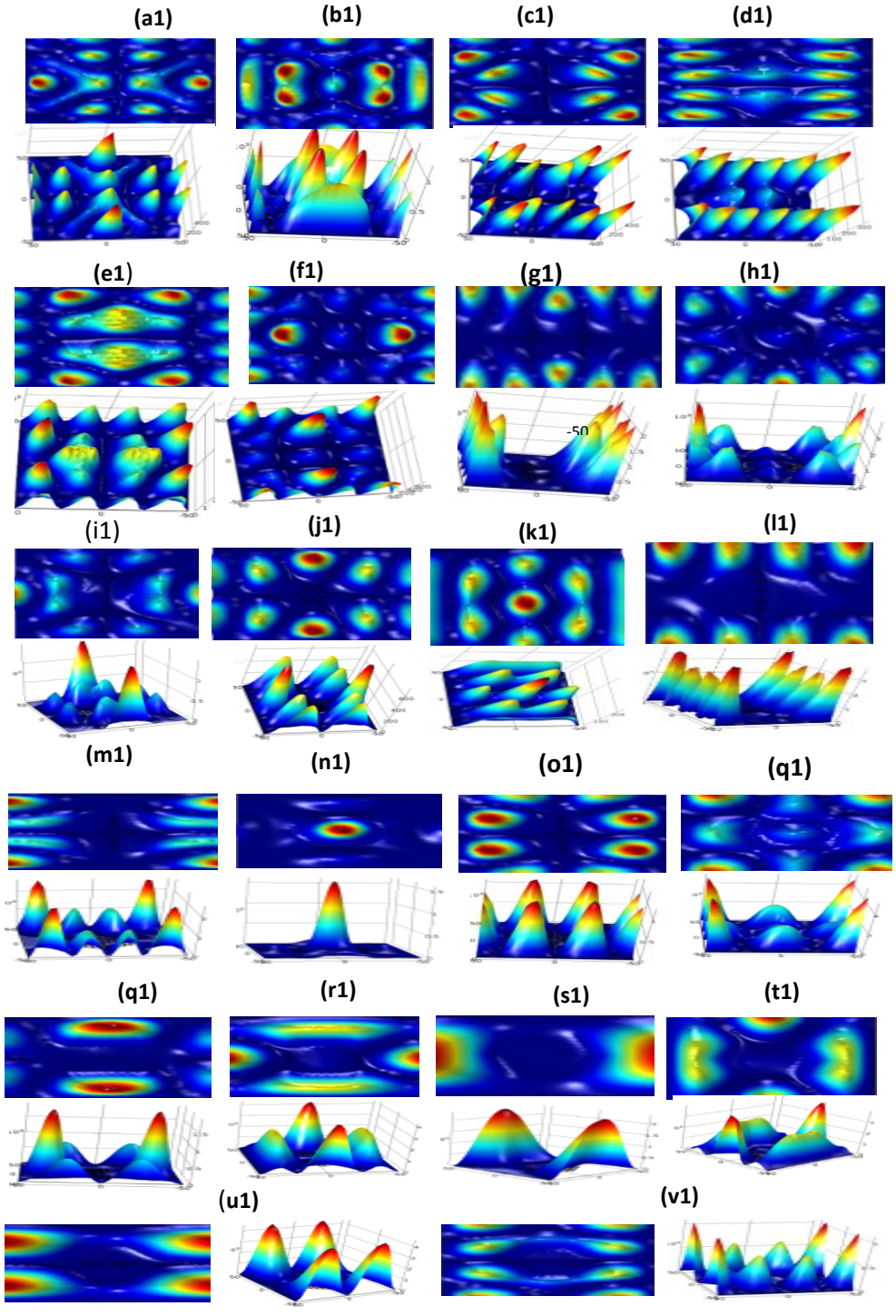

(B)

Fig. (3) Distributions of field model for TE (A) and TM (B) polarization modes for 2D (up), 3D (down) depressed cladding PC $LiNbO_3$ with pitch Λ=5μm at the wavelength 1.55μm, the model distributions are single and multimode for the extraordinary and ordinary polarizations, where (f, g, h, l, m, o, r, s, t , u and v) and in (f1, g1, h1, l1, m1, o1, r1,s1,t1 ,u1 and v1) are along the E polarization index (n_e) whereas other polarization are along the O index (n_o), the variation of the refractive index of the E polarization is less than that of the O polarization in both cases, this indicates slightly strong guiding properties along O than E polarizations

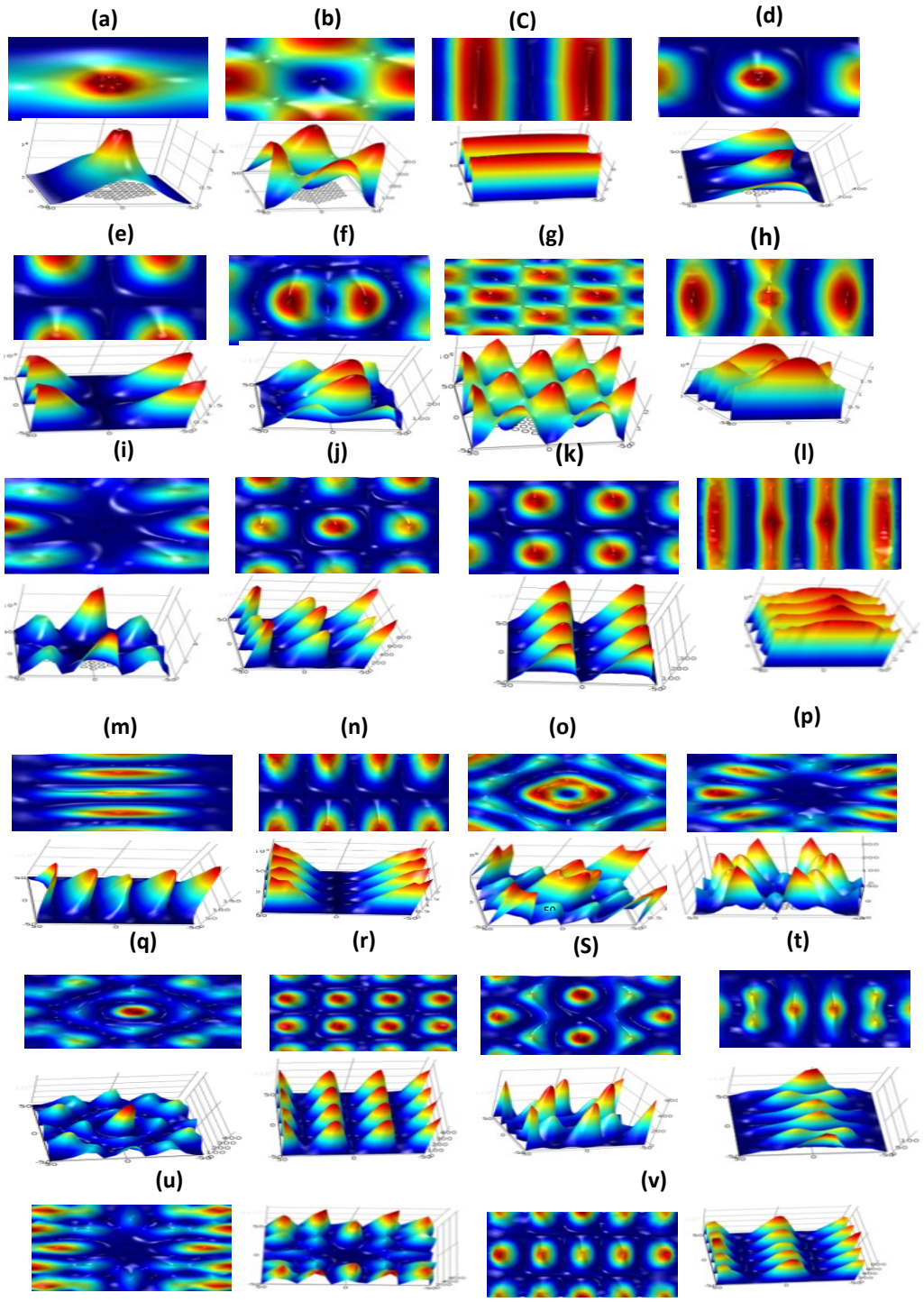

(A)

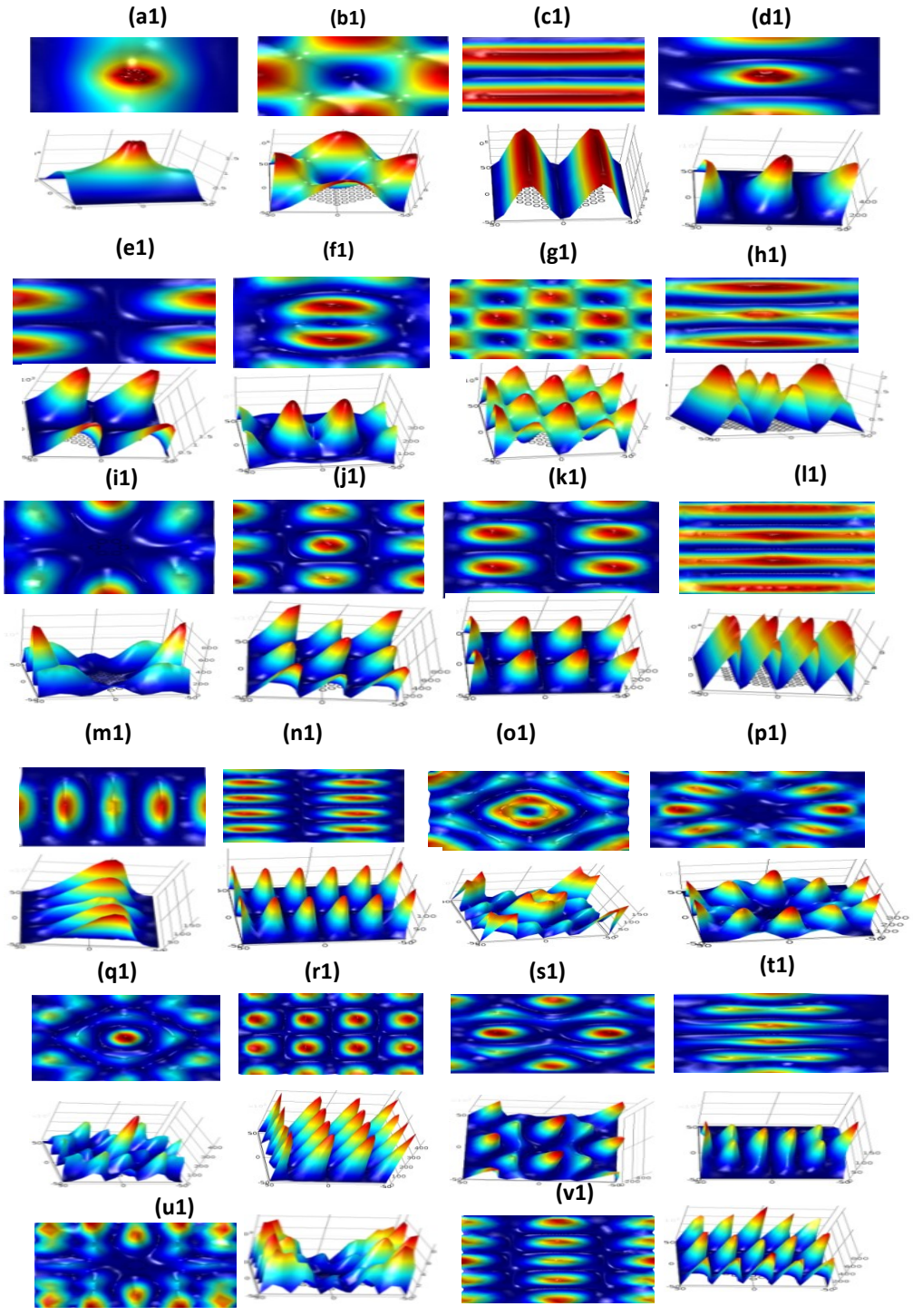

(B)

Fig. (4) Distributions of field model of the TE (A) and TM (B) polarizations for 2D depressed cladding PC $LiNbO_3$ with pitch Λ=7μm at the wavelength 1.55μm, the model distributions at (b, e , k, i ,n, p, s and u) and (b1, e1, k1, i1,, n1 , p1, s1 and u1) are along the E polarization index (n_e), whereas other polarized modes are along the O polarization index (n_o), the variation of the refractive index of the E polarization is less than that of the O polarization in both cases, this indicate slightly strong guiding properties along O than E polarizations

